Wang et al. *Cell Discovery* (2023)9:11
https://doi.org/10.1038/s41421-022-00511-1

Cell Discovery
www.nature.com/celldisc

ARTICLE Open Access

Chromosome territory reorganization through artificial chromosome fusion is compatible with cell fate determination and mouse development

Yuang Wang[1], Zhen Qu[2], Yi Fang[2], Yulong Chen[2], Jiayin Peng[1], Jiawen Song[1], Jinsong Li[1,3,4], Jiantao Shi[2], Jin-Qiu Zhou[2,3,4]✉ and Yun Zhao[1,3,4]✉

Abstract

Chromosomes occupy discrete spaces in the interphase cell nucleus, called chromosome territory. The structural and functional relevance of chromosome territory remains elusive. We fused chromosome 15 and 17 in mouse haploid embryonic stem cells (haESCs), resulting in distinct changes of territories in the cognate chromosomes, but with little effect on gene expression, pluripotency and gamete functions of haESCs. The karyotype-engineered haESCs were successfully implemented in generating heterozygous (2n = 39) and homozygous (2n = 38) mouse models. Mice containing the fusion chromosome are fertile, and their representative tissues and organs display no phenotypic abnormalities, suggesting unscathed development. These results indicate that the mammalian chromosome architectures are highly resilient, and reorganization of chromosome territories can be readily tolerated during cell differentiation and mouse development.

Introduction

Chromosome is the main carrier of genetic information, and is responsible for the transmission of genetic materials from parents to offspring. The number of chromosomes found in natural eukaryotic species ranges from one to thousands[1,2]. In most eukaryotic cells, chromosomes appear as chromatin during the interphase of the cell cycle and as linear "rods" during the mitotic phase[3]. For a chromosome to function stably and effectively across generations, it must have a centromere and two telomeres. Centromere is a specific locus on a chromosome for assembly of the kinetochore, which is responsible for microtubule attachment and precise chromosome segregation during cell division[4], while telomeres are the physical ends of a chromosome that protect the chromosome from degradation[5,6].

Chromosomes do not seem to be randomly distributed or intermingled with each other in the nucleus. Instead, each chromosome occupies a distinct spatial volume in the interphase nucleus, called chromosome territory[7–10]. In addition, the territory of a particular chromosome may be different in different cell types[7,11,12]. Accordingly, a proximal positioning of adjacent chromosomes may also be meaningful, e.g., regulating chromatin activities[13–15]. But what determines chromosome territory and how it regulates genome function are unclear.

The chromosome number in naturally evolved house mice *Mus musculus domesticus*, which have populated in Western Europe and North Africa, ranges from 2n = 40 to 2n = 22[16–18]. Some of their chromosomes are metacentric, i.e., the centromere is at the middle of each chromosome due to fusions of two telocentric chromosomes, which are commonly found in the laboratory

Correspondence: Jin-Qiu Zhou (jqzhou@sibcb.ac.cn) or
Yun Zhao (yunzhao@sibcb.ac.cn)
[1]State Key Laboratory of Cell Biology, Shanghai Institute of Biochemistry and Cell Biology, Center for Excellence in Molecular Cell Science, Chinese Academy of Sciences, University of Chinese Academy of Sciences, Shanghai, China
[2]State Key Laboratory of Molecular Biology, Shanghai Institute of Biochemistry and Cell Biology, Center for Excellence in Molecular Cell Science, Chinese Academy of Sciences, University of Chinese Academy of Sciences, Shanghai, China
Full list of author information is available at the end of the article

mouse (e.g., C57BL/6)[19]. In addition, Muntjac deer (Muntiacus, Muntiacinae, Cervidae) have evolved quite diverse karyotypes (e.g., 2n = 46 of *M. reevesi* and 2n = 6/7 of *M. muntjak vaginalis*) through chromosome translocation, tandem fusion, and pericentric inversion[20–22]. Recently, deliberate artificial chromosome engineering has succeeded in generating single-chromosomal *Saccharomyces cerevisiae* and *Schizosaccharomyces pombe* strains, which show drastic changes in global chromosome structures, but grow as robustly as the naturally evolved strains[23–25]. These lines of evidence suggest that chromosome architecture in eukaryotes is highly resilient, and chromosome territories could be self-organizing representations of the genome, or simply be a manifestation of random chromatin collisions driven by intrinsic interactions between chromatin loci and/or geometric constraints within the nucleus.

In order to experimentally address whether the high plasticity of chromosome architecture is a ubiquitous characteristic of eukaryotic genomes, we employed haploid embryonic stem cells (haESCs) and mouse models to test the effects of extreme chromosome territory changes on stem cell pluripotency, cell fate determination and mouse development.

Results

Construction of chromosome fusion haESCs

We used CRISPR-Cas9 to induce double-strand-breaks in chromosome 15 (Chr15) and chromosome 17 (Chr17) in mouse haESCs, namely H19ΔDMR-IGΔDMR-AGH (hereafter referred as WT)[26]. The guide RNA (gRNA) targeting sites were in the regions of distal telomere (D-telomere) region of Chr15 and sub-centromeric telomere (C-telomere) region of Chr17, respectively (Fig. 1a; Supplementary Fig. S1a). The broken chromosomes might fuse together by non-homologous-end joining (NHEJ) (Fig. 1a), an active DNA repair mechanism intrinsic to cells [27].

The haESCs were transfected with CRISPR-Cas9 vectors, and potential clones were screened by cross-chromosomal PCR using primer pairs ~400 bp upstream and ~250 bp downstream of the respective gRNA targeting sites in Chr15 and Chr17 (Fig. 1a). Two clones namely 25A and 42E showed an amplified band with the expected length (Fig. 1b; Supplementary Fig. S1b). Further sequencing results confirmed that both PCR products matched the sequences adjacent to the respective gRNA targeting sites in Chr15 and Chr17 (Supplementary Fig. S1c), with 9 bp and 7 bp deletion at the junction sites, respectively, indicating that chromosome fusion in both clones is likely mediated by NHEJ.

Next, we performed chromosome fluorescence in situ hybridization (FISH) analysis by employing whole painting probes to verify chromosome fusion at the cellular level. In WT haESCs, the Chr15 and Chr17 were labeled with red and green fluorescent probes, respectively. In 25A and 42E cells, one half of a chromosome was labeled with red fluorescence, while the other half was labeled with green fluorescence, indicating the fusion of Chr15 and Chr17 (Fig. 1c; Supplementary Fig. S1d). Notably, in either 25A or 42E cell line, there was a mini-chromosome (indicated by the white arrowhead in Fig. 1c and Supplementary Fig. S1d) that was not seen in the WT haESCs. We speculated that this mini-chromosome was the abandoned C-telomere of Chr17, and was stably maintained during the passages of the haESCs. Consistently, karyotype analysis also showed that Chr15 and Chr17 were fused (the red arrowhead in Supplementary Fig. S1e, f), and the mini-chromosome was retained in 25A and 42E cells (the blue arrowhead in Supplementary Fig. S1e, f).

Chromosome fusion in haESCs does not affect cell pluripotency

To address whether chromosome fusion in haESCs affects cellular functions, we examined cell morphology, proliferation rate, karyotype stability and differentiation potentials. We isolated the haploid (G0/G1 phase) 25A cells by fluorescence-activated cell sorting (FACS) (Supplementary Fig. S2a), and there was no significant difference between 25A and WT in terms of proliferation rate and colony morphology (Fig. 1d; Supplementary Fig. S2b), and the karyotype of 25A was stably maintained after 25 passages (Supplementary Fig. S2c, d), suggesting that chromosome fusion does not affect mitosis.

Chromosome fusion 25A cells expressed pluripotency marker genes, including *Oct4*, *Sox2* and *Nanog*, which were not significantly different from WT (Supplementary Fig. S2e). To assess whether 25A cells remain pluripotent, we induced in vitro differentiation by removing leukemia inhibitory factor (LIF) and two differentiation inhibitors (CHIR99021, PD0325901) in the culture medium (Supplementary Fig. S2f). The cells showed differentiation morphology after two weeks (Supplementary Fig. S2g), in coincidence with the downregulation of pluripotency marker genes and the upregulation of the three germ layers' differentiation-related genes (Ectoderm marker genes: *Pax6*, *Nestin*; Mesoderm marker genes: *KDR*, *αSMA*, *PDGFRα*; Endoderm marker genes: *AFP*, *Gata4*, *Gata6*) (Fig. 1e). Furthermore, subcutaneous injection of 25A cells into immunodeficient mice resulted in the formation of teratomas, which contained three germ layers identified by immunohistochemistry (IHC) (Fig. 1f). Collectively, these results indicate that chromosome fusion in haESCs does not affect cell pluripotency.

Chromosome fusion leads to rearrangement of chromosome territory

There have been indications that different chromosomes occupy different spaces in cell nucleus, and the

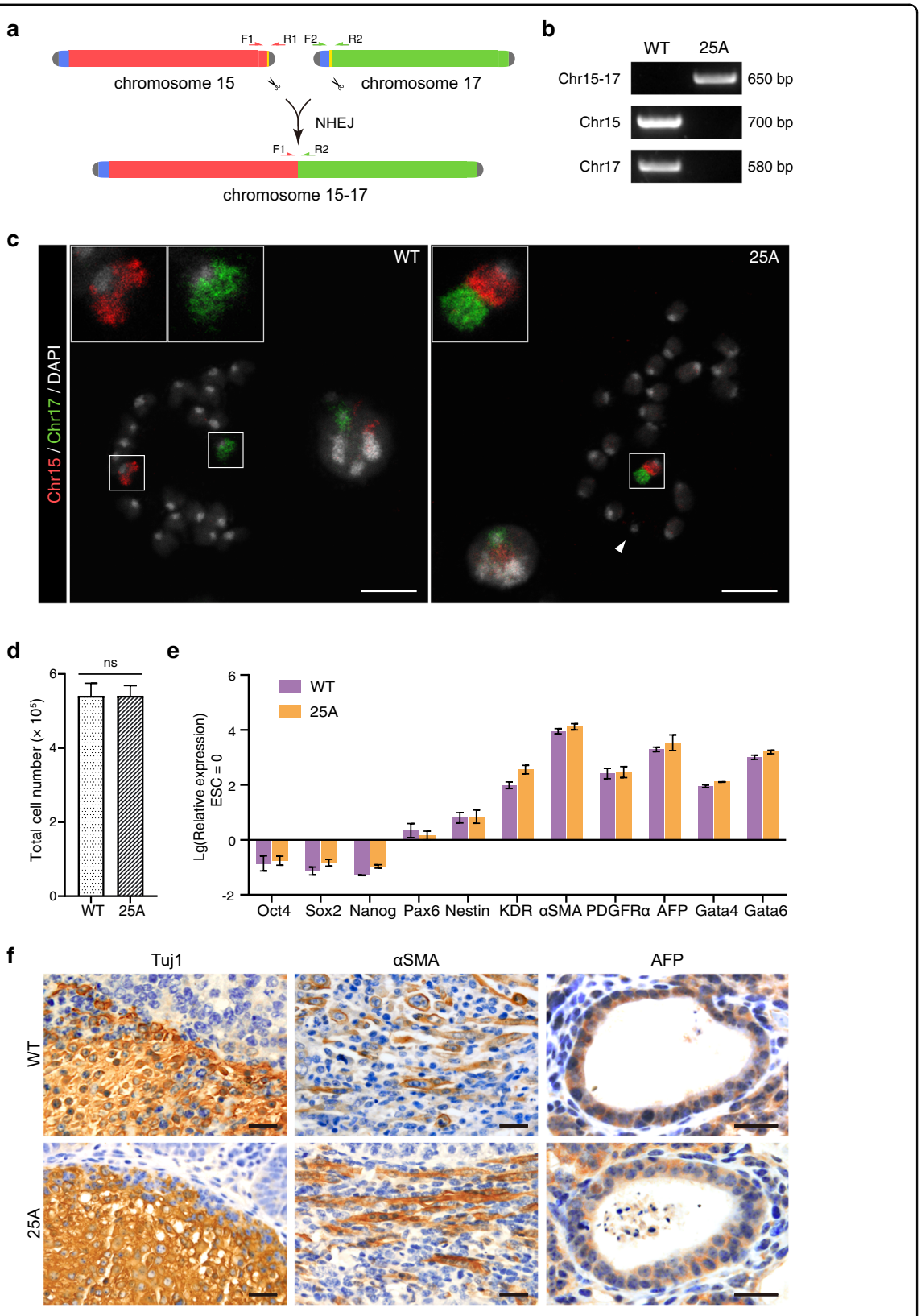

Fig. 1 (See legend on next page.)

(see figure on previous page)
Fig. 1 CRISPR/Cas9 mediated site-specific chromosome breaks and Chr15-17 fusion in haESCs. a Schematic showing the experimental strategy for generating site-specific chromosome fusion of Chr15 (red) and Chr17 (green) in haESCs. Two sgRNAs guide Cas9 (scissors) to the indicated target sites (yellow) located near D-telomere region (gray) of Chr15 and C-telomere region (blue) of Chr17, respectively. Chromosome fusion occurred between two target sites and was detected by cross-chromosomal PCR. Chr15 without D-telomere and Chr17 without C-telomere are ligated through NHEJ pathway, generating Chr15-17 fusion. Primers are designed at the upstream and downstream of each sgRNA target site. **b** PCR analysis of 25A haESCs with primers mentioned in (**a**). Cross-chromosomal PCR with primer pairs 'F1' and 'R2' amplified a ~ 650 bp band only in 25A, while "F1" and "R1" on Chr15 and "F2" and "R2" on Chr17 amplified a ~700 bp and a ~580 bp band, respectively only in WT but not in 25A. **c** Fluorescent images of the metaphase chromosomes of WT and 25A haESCs labeled with whole painting probes of Chr15 (red) and Chr17 (green). Insets zoomed-in showing the Chr15 and Chr17 in WT and the fused Chr15-17 in 25A. The mini-chromosome is indicated with a white arrowhead. Scale bar: 10 μm. **d** Proliferation rates examined by total cell number of WT and 25A haESCs. ns not significant. **e** Real-time PCR analysis of the expression levels of pluripotency marker genes (*Oct4*, *Sox2* and *Nanog*) and differentiation-related genes (Ectoderm: *Pax6, Nestin*; Mesoderm: *KDR, αSMA, PDGFRα*; Endoderm: *AFP, Gata4, Gata6*) in differentiated WT and 25A cells. The expression levels were Log transformed. Data are represented as the mean ± SD, $n = 3$. Gene expression levels were not significant between WT and 25A cells. **f** Paraffin sections of teratomas formed by WT and 25A cells were stained with three germ-layer markers including the ectoderm marker Tuj1, the mesoderm marker αSMA and the endoderm marker AFP. Scale bar: 20 μm.

adjacent positioning of chromosomes suggests that their interactions are significant[7]. To explore the effect of chromosome fusion on chromosome territories, we performed whole-genome chromosome conformation analysis on diploid 25A and WT cells with high-coverage Hi-C sequencing (~100×). In the genome-wide contact matrixes, the inter-chromosomal interactions of Chr15 and Chr17 were largely random in WT cells (Fig. 2a; Supplementary Fig. S3a, c, e), while significantly enhanced in 25A cells, presumably because the fusion of two chromosomes resulted in the significant emergence of new intra-chromosome interactions (Fig. 2a; Supplementary Fig. S3b, d, f). The distribution of contact probabilities as a function of genomic distances in fused Chr15-17 is indistinguishable from that of a single chromosome (e.g., Chr1 in WT or 25A) (Fig. 2b), indicating that chromosome fusion has not only disrupted the original territories of native Chr15 and Chr17, but also established a new territory in the fused chromosome.

In addition, based on the Hi-C results, we inferred the consensus 3D structure of the genome in both WT and 25A cells (Fig. 2c; Supplementary Videos S1, S2). Notably, Chr15 and Chr17, which were separated in WT, clustered together in 25A. Moreover, the territory of Chr17 underwent an outward shift toward nucleus periphery to near the location of Chr15 in 25A compared to WT, indicating that the radial position of the Chr17 relative to the center of the nucleus also changed significantly after chromosome fusion. Interestingly, most of the chromosomes stayed in their radial positions, but a few chromosomes showed radial displacements, such as Chr9 moved outward while Chr12 and Chr16 shifted inward (Fig. 2d), which were likely a result of the disturbance caused by redistribution of Chr15-17 territory. Further 3D-FISH analysis in 25A cells consistently showed a juxtaposition of Chr15 (labeled with red) and Chr17 (labeled with green), an indication of a single territory of the fusion chromosome (Fig. 2e). Statistical analysis also revealed that Chr15 and Chr17 clustered together in 25A and the radial position of Chr17 in the nucleus was shifted outward (Fig. 2e, f). Notably, within the new single chromosome territory formed by fused Chr15-17, there was no extensive intermingling between the two moieties of Chr15 and Chr17 (Fig. 2e), suggesting that a chromosome territory is not chaotically arranged, but rather likely determined by continuous DNA sequences and cis-interactions between chromatin loops or topologically associating domains (TADs) within each chromosome.

Previous studies have suggested that larger chromosomes are more likely to be distributed at the periphery of the nucleus, while the shorter chromosomes tend to be located in the center[3,12,14,28–30]; the chromosome with higher and lower gene density are respectively located at the center and the edge of the nucleus[12,28,30,31]. Consistent with previous reports, the fusion of Chr15 and Chr17 which are relatively short among the mouse native chromosomes increased the chromosome size (even longer than the largest Chr1) in 25A (Supplementary Fig. S3g–i), and the fusion chromosome is located at the edge of the nucleus (Fig. 2d; Supplementary Fig. S3j). The radial position of a chromosome and gene density is negatively correlated in WT cells ($P = 0.015$). However, this correlation is disrupted in 25A ($P = 0.158$) (Supplementary Fig. S3i, k). The gene density of fused Chr15-17 was higher than the average gene density (Supplementary Fig. S3i, k), but it still moved outward, indicating a weak correlation between the radial position of a chromosome and gene density in mouse cells.

Chromosome territory rearrangement has little effect on gene expression

Chromosome territory as well as inter-chromosome interactions have been suggested to affect gene expression[32–35]. Thus, we performed RNA-seq and transcriptome analyses in 25A cells. To our surprise, although the fusion of Chr15 and Chr17 resulted in drastic changes

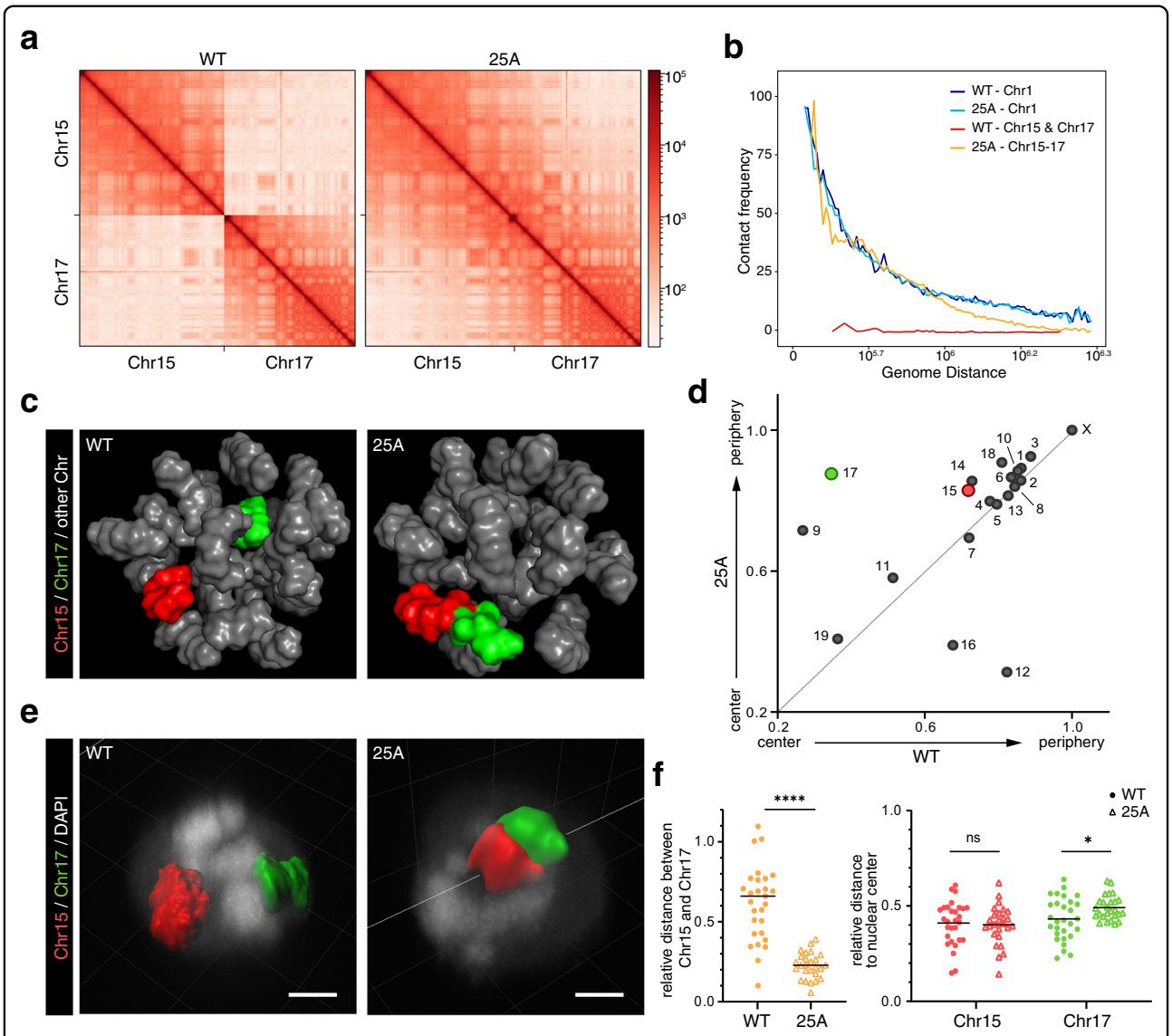

Fig. 2 Change of chromosome territory after Chr15 and Chr17 fusion. a Contact matrixes at 1 Mb resolution on Chr15 and Chr17 of WT and 25A cells. **b** Contact frequency curves showing contact probabilities as a function of genomic distances around fusion site (within 1 Mb) on Chr15 and Chr17. Chr1 was included as a single chromosome control. **c** Inferred 3D genome structures in WT and 25A cells using Hi-C data. Chr15 was shown in red and Chr17 in green. **d** Radial distributions of each chromosome relative to nucleus center in WT (horizontal axis) and 25A (vertical axis) derived from inferred 3D models (**c**). **e** 3D-FISH reconstruction of the Chr15 and Chr17 in WT and 25A haESCs. Chr15 was labeled in red and Chr17 in green. Scale bar: 2 μm. **f** Quantification of relative distance between Chr15 and Chr17 (left), and relative distance of Chr15 and Chr17 to the nucleus center (right) in WT and 25A haESCs. (mean ± SD, two-tailed ratio Student's *t*-test, $^{*}P < 0.05$, $^{**}P < 0.01$, $^{***}P < 0.005$, $^{****}P < 0.0001$, ns not significant. $n = 29$ and 26 cells, respectively).

in both the relative positions and the radial distributions of chromosome territories, these perturbations exerted no apparent effects on global gene expression. Compared to WT cells, only 0.33% of the genes in the whole genome of 25A cells displayed significant differential expression (FDR < 0.05, $\log_2$(FC) > 0.5) (Fig. 3a; Supplementary Fig. S4a, b), most of which (94.8%) had an expression difference of less than twofold (Supplementary Fig. S4c). Interestingly, there was no correlation between the distribution of differentially expressed genes and the specific changes of chromosomal territories on Chr15 and Chr17 (Fig. 3b; Supplementary Fig. S4d). These results indicated that the rearrangement of chromosome territories by chromosome fusion imposes little effect on gene expression.

The loose link between the significant reorganizations of chromosome territories and the subtle changes of gene expressions prompted us to ask whether chromosome

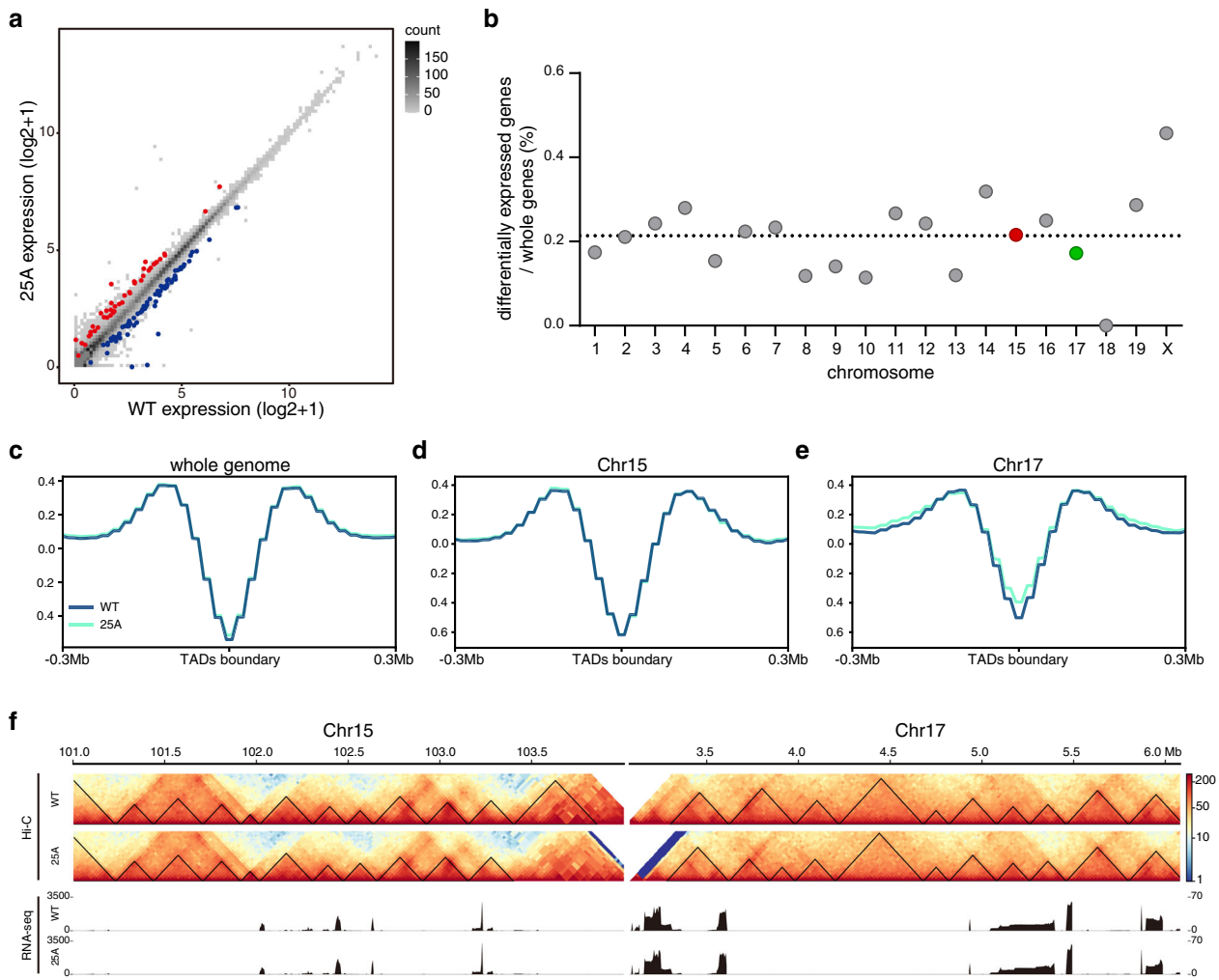

Fig. 3 Transcriptome and TADs analyses in 25A cells. a Comparison of gene expression in 25A cells and WT cells. Upregulated and downregulated genes were shown in red and blue, respectively (FDR < 5%). **b** The proportion of the differentially expressed genes in each chromosome of 25A cells. The dash line indicates the average proportion of differentially expressed genes of the whole genome. **c**–**e** Comparison of TAD boundaries in WT and 25A cells. Aggregate profiles of insulation scores around TADs boundaries at a 10 Kb resolution for the whole genome (**c**), Chr15 (**d**) and Chr17 (**e**). **f** Hi-C contact matrixes of the 3 Mb region upstream from chromosome fusion site on Chr15 and downstream on Chr17 of WT and 25A cells. TADs are depicted as black triangles. RNA-seq expression tracks in the corresponding fusion regions in both WT and 25A cells are shown in lower panels.

fusion affected the lower levels of chromatin architecture, e.g., TADs, since TADs have been considered to be the functional units that regulate gene expression[36–38]. Therefore, we further analyzed TADs in the whole genomes of both WT and 25A cells, and found that the insulation score near TADs boundaries across whole genome, including Chr15 and Chr17 in the WT cells and Chr15-17 in the 25A cells were indistinguishable (Fig. 3c–e), indicating that the changes of chromosome territories did not disturb the overall TADs. Surprisingly, compared to that in WT, TADs within the 6 Mb fusion regions of Chr15 and Chr17 in 25A remained largely unchanged (Fig. 3f, upper panels), providing a plausible explanation for nearly the identical gene expression patterns within the fusion regions in the WT and 25A cells (Fig. 3f, lower panels).

Generation of chromosome fusion mice

Chromosome territories appear to be different in different cell types[28,39], suggesting that there are functional correlations between chromosome architecture (chromosome interaction) and gene expression. In order to explore further the effect of chromosome-fusion-induced changes of chromosome territory at the organismal level, we audaciously injected 25A haESCs into WT mouse oocytes through intracytoplasmic AG-haESC injection

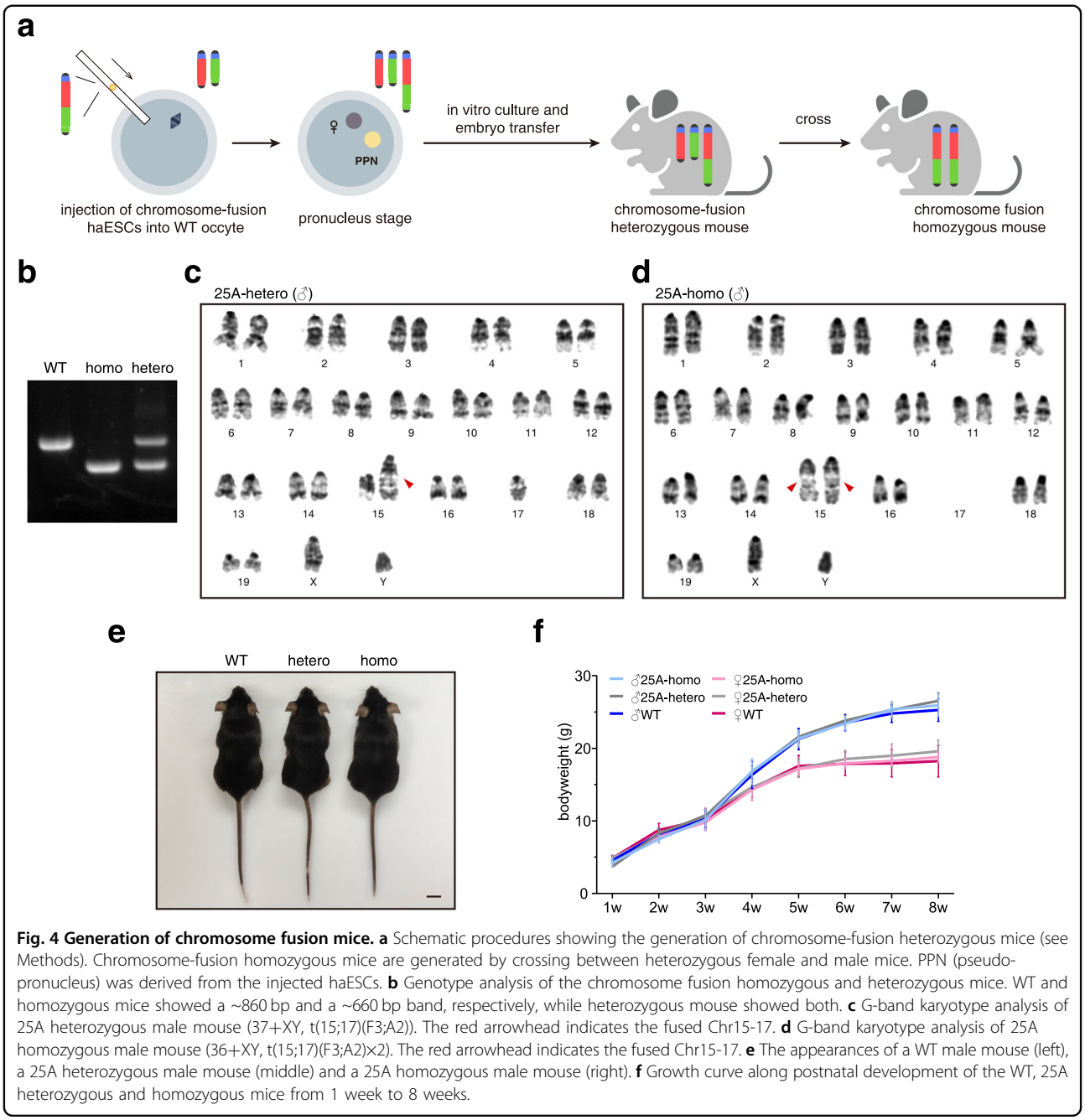

Fig. 4 Generation of chromosome fusion mice. a Schematic procedures showing the generation of chromosome-fusion heterozygous mice (see Methods). Chromosome-fusion homozygous mice are generated by crossing between heterozygous female and male mice. PPN (pseudo-pronucleus) was derived from the injected haESCs. **b** Genotype analysis of the chromosome fusion homozygous and heterozygous mice. WT and homozygous mice showed a ~860 bp and a ~660 bp band, respectively, while heterozygous mouse showed both. **c** G-band karyotype analysis of 25A heterozygous male mouse (37+XY, t(15;17)(F3;A2)). The red arrowhead indicates the fused Chr15-17. **d** G-band karyotype analysis of 25A homozygous male mouse (36+XY, t(15;17)(F3;A2)×2). The red arrowhead indicates the fused Chr15-17. **e** The appearances of a WT male mouse (left), a 25A heterozygous male mouse (middle) and a 25A homozygous male mouse (right). **f** Growth curve along postnatal development of the WT, 25A heterozygous and homozygous mice from 1 week to 8 weeks.

(ICAHCI), and the resulting embryos were implanted into the uterus of surrogate mother mice (Fig. 4a). Like the WT haESCs, 25A haESCs were functioning as "sperms", and yielded heterozygous F0 female mouse, whose cells contained both the fusion Chr15-17 and the native Chr15 and Chr17 (Supplementary Fig. S5a). Karyotype analysis of the bone marrow cells confirmed that the F0 female mouse had a fused Chr15-17 and the mini-chromosome, which existed in 25A cell line (Supplementary Fig. S5b). The appearance and growth of F0 heterozygous female mice were not significantly different from the mice generated in parallel with WT haESCs through the ICAHCI method. We then examined the reproductive capability of F0 female mice by both in vitro fertilization and natural cross-breeding with WT males, respectively, and both methods produced healthy F1 offspring with approximately 1:1 ratio of heterozygous to WT mice (Supplementary Fig. S5c), which fits the Mendelian genetics well. Interestingly, the mini-chromosome seen in the F0 mice was absent in heterozygous F1 mice (Fig. 4c; Supplementary Fig. S5d), indicating that the mini chromosome was lost during breeding F1 mice.

The mini-chromosome loss was not surprising because it mainly contained the telomere and centromere sequences, in which there were no essential genes. We speculate that the mini-chromosome may not segregate properly into the oocyte due to the lack of homologous chromosome to pair with during meiosis in F0 germ cells. These results indicate that the Chr15-17 fusion is "overlooked" by the zygotes, and as a result, the heterozygous female mice are still fertile though the litter size (3.50 ± 1.38, $n = 6$) is smaller than WT (6.22 ± 2.33, $n = 9$) (Supplementary Fig. S5e).

We took a step further to cross heterozygous mice and obtained homozygous mice containing two copies of the fusion chromosomes (Fig. 4a, b). Mating male and female heterozygous mice exhibited a reduced litter size (2.76 ± 1.67, $n = 21$) (Supplementary Fig. S5e), but the percentage of WT (23.3%), heterozygous (55.9%) and homozygous (20.7%) pups appears to fit the Mendelian genetics (Supplementary Fig. S5f), suggesting fusion of chromosome has little effect on gamete viability, fertilization and embryonic development. Karyotype analysis of the homozygous mice showed two fused Chr15-17 (Fig. 4d; Supplementary Fig. S5g). Apparently, homozygous, heterozygous and WT mice showed no differences in appearance, postnatal growth and development (Fig. 4e, f). Homozygous male and female mice can produce homozygous offspring, and their reproductivity (5.45 ± 1.86, $n = 11$) is nearly the same as that of WT mice (Supplementary Fig. S5e). These results indicate that chromosome fusion has no obvious effect on the growth, development and reproduction of mice.

Chromosome territory rearrangement by chromosome fusion causes no detectable defects in mouse tissues or organs

We then examined the effects of chromosome fusion on the functions of different tissues and organs in homozygous and heterozygous mice. The shape and weight of the main organs (such as liver, spleen and lung) in the heterozygous and homozygous mice were very similar to those of WT mice (Fig. 5a–d; Supplementary Fig. S6a, b). Additional Hematoxylin & Eosin (HE) staining showed that both the internal structure and the constitutions of the main organs (liver, spleen, lung, heart and kidney) as well as reproductive organs (testis and ovary) matched well with those of WT mice (Fig. 5e; Supplementary Fig. S6c–e). Further chromosome FISH on the cells of several organs revealed that in homozygous mice, the Chr15-17 fusion was intact, and the rearranged chromosome territories were different from those observed in the cells from WT organs (Fig. 5f, g). Notably, the radial position of Chr15-17 showed an outward shift in spleen cells, but no significant movement in liver and lung cells (Fig. 5f, h), consistent with the notion that a given chromosome in different cell types may display different territories[7,11,12]. Regardless of cell-type differences, within the single territory of fused Chr15-17, the moieties of Chr15 and Chr17 distal to the fusion regions did not mingle with each other (Fig. 5f), further supporting the model that a chromosome territory is primarily determined by continuous DNA sequences and the cis-interaction between chromatin loops or TADs with special proximity. At the metabolic level, the blood parameters, including complete blood count and serum biochemical test, were analyzed and found no significant differences between WT and chromosome-fusion mice (Fig. 5i; Supplementary Table S1). We thus concluded that the rearrangements of chromosome territories by chromosome fusion do not cause detectable defects in mouse cell differentiation, organogenesis and development.

Discussion

There are forty chromosomes in the diploid of mouse cells, nineteen pairs of autosomes (from Chr1 to Chr19) and two sex chromosomes (ChrX and/or ChrY). The autosomes are likely numbered according to their size: Chr1 is the longest (195 Mb), and Chr19 is the shortest (62 Mb). The lengths of X and Y chromosomes are 169 Mb and 91 Mb, respectively (Supplementary Fig. S3i). Mouse autosomes are all telocentric, i.e., the centromere of the chromosome is located next to one of the telomeres (Supplementary Fig. S1a). Though the DNA in both centromeric and telomeric regions are repetitive sequences[40,41], the primary structure of a centromere consists of minor satellite and major satellite, and is much more complicated than that of a telomere, which mainly consists of regular $(TTAGGG)_n$ repeats (Supplementary Fig. S1a)[41]. The telomere-centromere layout of mouse chromosomes facilitates chromosome engineering: deletions of both centromere and the proximal telomere in a given chromosome can be done at one CRISPR-Cas9 cut (Fig. 1a; Supplementary Fig. S1a). However, poor annotations of the genes near each centromeric region lead to potential uncertainties of chromosome fusion. We first carefully analyzed all of the genes near centromere in every chromosome, and found that some of the chromosomes, such as Chr13, Chr15, Chr16 and Chr17 are suitable candidates for chromosome fusion. Second, chromosome size after fusion could be potentially problematic, because there might be a length limit that a cell can tolerate[42–44]. Third, the radial distribution of chromosome territories in the nucleus has been proposed to be correlated with chromosome length and gene density[12,28,30,31]. Chromosomes with larger size and lower gene density tend to be distributed at the periphery of the nucleus, and vice versa. Given that (1) Chr15 and Chr17 are relatively small, and their fusion results in a 199 Mb chromosome, which is slightly longer than the largest

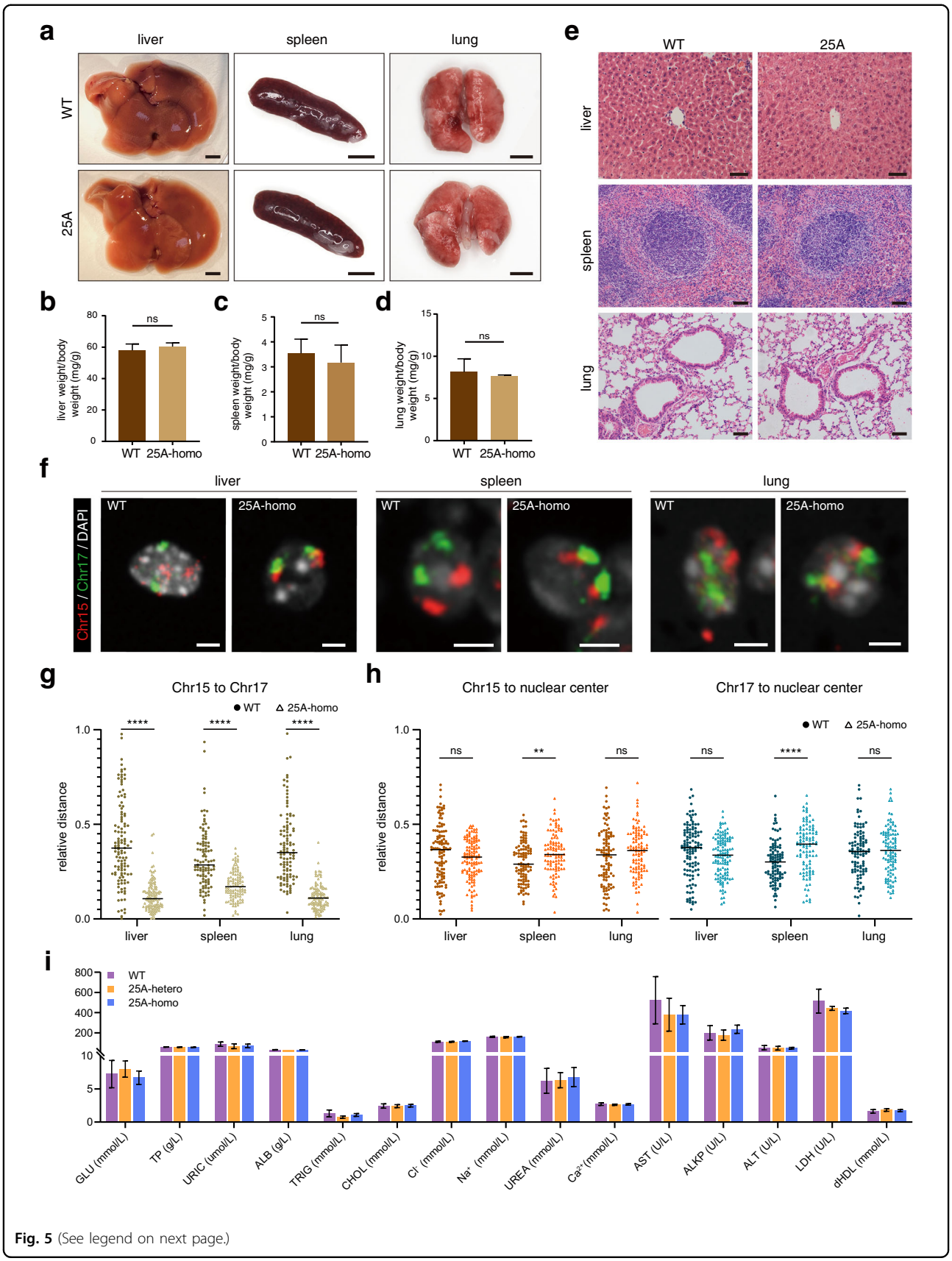

Fig. 5 (See legend on next page.)

(see figure on previous page)
Fig. 5 Phenotypic analyses of chromosome fusion mice. a Morphological features of liver, spleen and lung from adult WT and 25A (Chr15-17 fusion) homozygous mice. Scale bar: 300 mm. **b**–**d** Relative organ weight to body weight of liver (**b**), spleen (**c**) and lung (**d**) in 8 weeks WT and Chr15-17 fusion homozygous mice. (mean ± SD, two-tailed Student's *t*-test, $n = 3$). **e** HE staining of liver, spleen and lung from 8 weeks WT and Chr15-17 fusion homozygous mice. Scale bar: 50 μm. **f** Chromosome FISH for Chr15 (red) and Chr17 (green) in the cells of liver (left), spleen (middle) and lung (right) from WT and Chr15-17 fusion homozygous mice. The nuclei were stained with DAPI (gray). Scale bar: 2.5 μm. **g** Quantification of relative distance between Chr15 and Chr17 in the cells of the corresponding organs of WT and Chr15-17 fusion homozygous mice. (two-tailed Student's *t*-test, $n = 118$, 120, 102, 102, 104 and 104 chromosomes, respectively.) **h** Quantification of relative distance of Chr15 and Chr17 to the nucleus center in the cells of the corresponding organs of WT and Chr15-17 fusion homozygous mice. (two-tailed Student's *t*-test, $n = 118$, 120, 102, 102, 104 and 104 chromosomes, respectively.) **i** Serum biochemical test of WT, Chr15-17 fusion heterozygous and homozygous mice. (mean ± SD, $n = 5$, 3, 3 mice, respectively).

Chr1 (195 Mb) (Supplementary Fig. S3i); (2) the gene density of Chr17 is significantly higher, while the gene density of Chr15 is lower than that of other chromosomes, and the fused Chr15-17 displays a medium gene density between the Chr15 and Chr17 (Supplementary Fig. S3i), we have chosen Chr15 and 17 to perform chromosome fusion. In spite of these concerns, the successful construction of fusion chromosome implies that reconstruction of mouse genome might not be an impossible task.

The eukaryotic genome seems to have evolved into a hierarchical structure, including chromatin loops, TADs, compartments and chromosome territories[9,10,45]. The driving forces for these hierarchical arrangements are still mysterious. It has been proposed that chromosome territory regulates genome architecture and thereby affects gene expression[32–35]. However, in the single cell organisms like *S. cerevisiae* and *S. pombe*, drastic chromosome architecture changes by artificial chromosome engineering cause marginal changes in gene expressions and affect little the functions of yeast cells[23–25]. In addition, the chromosome fusion in haESCs results in chromosome distribution changes in cell nucleus, but neither induces obvious genome instability, nor causes detectable defects in gene expression, pluripotency and gamete function (Figs. 1–3). Importantly, the mice containing the fusion chromosome are apparently healthy, and competent to propagate regardless of the chromosome territory perturbations in various cell types of individual tissues and organs (Figs. 4–5). These lines of evidence strongly suggest that the territories of individual chromosomes in the eukaryotic nucleus might be passively demarcated under the scenarios of geometric constraints and chromatin collisions in the limited volume of cell nucleus, and the effects of chromosome territories on gene expression are generally insignificant or even dispensable. However, there are cases that trans-interactions between two chromosomes are functional[15,46,47], suggesting coincidences of evolution. Nevertheless, the chromosome fusion does not seem to change TADs of the corresponding chromosomes (Fig. 3c–e), consistently supporting the hypothesis that TADs are the functional units for the regulation of gene expression [36–38].

Different species on earth have different numbers of chromosomes. It remains elusive whether the genome organization in different species is randomly or fortuitously retained during the long course of evolution. We have arbitrarily fused Chr15 and Chr17 in haESCs, and fortunately cultivated the mice with $2n = 38$, indicating the high plasticity of mouse genome. The Chr15-17 fusion disturbs the radial positions of territories of the natural Chr15 and Chr17 (Fig. 2c–f), as well as Chr9, Chr12 and Chr16, but not others (Fig. 2d). Why and how the regional territory perturbations only affect some of the chromosomes remains unclear. In addition, we do not know whether the haESCs used in this work are able to tolerate additional chromosome fusions, and still able to maintain their pluripotency and gamete functions afterwards. Ideally, more dramatic changes of chromosome territories rely on more massive chromosome engineering, for example, to construct $n = 18$ (or even less) haESCs and/or mice through three-chromosome fusion or two-pairs of chromosome fusion. Coincidently, Wang et al. used the same approach as we did to engineer mouse chromosomes, and recently reported that the fusion of Chr4 and Chr5 did not affect the pluripotency of haESCs or embryogenesis, while the fusion of Chr1 and Chr2 in haESCs (two largest mouse chromosomes) resulted in mitotic defects[48], suggesting that there might be a length limit for appropriate chromosome function(s). Zhang et al. used the Robertsonian-fusion (centromere to centromere fusion) approach to engineer mouse chromosomes, and showed that the mice carried different pairs of chromosome fusion could be stably maintained and passaged in laboratory[49], reminiscent of the Robertsonian mice populated in Western Europe and North Africa[50]. These lines of evidence collectively support the conclusion that chromosome territory change induced by two-chromosome fusion can be negligible to cell fate determination and mouse development. Further extensive karyotype engineering will help to further clarify the structure-function correlations between chromosome territories and genome activities. But the global orchestration of genomic activities and regulations within the functional milieu of

the mammalian cell nucleus is so sophisticated that further extensive karyotype engineering might be extremely challenging.

Materials and methods

Animal use and care

All specific pathogen-free (SPF)-grade mice were maintained and handled in accordance with the ethical guidelines of the Center for Excellence in Molecular Cell Science, Chinese Academy of Sciences. C57BL/6 mice used for mating and propagation and BABL/c nude mice used for teratoma formation were obtained from Shanghai Jihui Laboratory Animal Care Company.

Cell culture

haESCs (H19ΔDMR-IGΔDMR-AGH) were maintained in a standard ESC culture system: DMEM (Millipore) with 15% FBS (Gibco), penicillin-streptomycin (Gibco), nucleosides (Millipore), non-essential amino acids (Millipore), L-glutamine (Millipore), β-mercaptoethanol (Millipore), 1,000 U/mL LIF(Millipore), 3 μM CHIR99021 (Selleck) and 1 μM PD03259010 (Selleck) [26,51–53].

FACS

haESCs were trypsinized into single cells and incubated with 15 μg/mL Hoechst 33342 (Invitrogen) in a 37 °C water bath for 5 min. The cell sorting was then conducted to harvest the haploid 1n peak by using FACS Aria II (BD Biosciences) [26,53–55].

CRISPR-Cas9 fused chromosomes in haESCs

The sgRNAs of Chr15 and Chr17 were connected to the pX330-mCherry plasmid (Addgene, 98750). WT cells were transfected with 250 μL Opti-MEM that contained 5 μL Lipofectamine 2000 (Thermo Fisher Scientific) and 2.5 μg sgRNA-pX330-mCherry plasmid. 20–48 h after transfection, haploid cells expressing red fluorescent protein were enriched by FACS and plated into one well of a 6-well plate at a low cell density of around 4000 cells per well. Single colony was picked and passaged to one well of a 96-well plate after 5–8 d. CRISPR-Cas9 target sites are listed in Supplementary Table S2.

Cell proliferation

Haploid cells enriched by FACS were collected to evaluate cell proliferation rate, 4.5×10^4 sorted cells were cultured in a well of a 24-well plate. After 3 d, cells were dissociated and counted.

ICAHCI and embryo transfer

ICAHCI and embryo transfer to generate mice were performed with the help of the Animal Core Facility, the Center for Excellence in Molecular Cell Science, Chinese Academy of Sciences as described previously [26,51].

Karyotype analysis and cell FISH

haESCs were incubated with 0.4 mg/mL demecolcine (Sigma) for 1 h. After trypsinization, the cells were resuspended in 0.075 M KCl at 37 °C for 15 min and then fixed in methanol: acetic acid (3:1 in volume) for 30 min. The cells were dropped onto pre-cold and precleaned slides.

For karyotype analysis, the protease-treated cells were stained with Giemsa dye (Yeasen) for 15 min. Pictures were taken by Olympus BX53 and more than 50 metaphase spreads were analyzed. The G-banded ideogram of chromosome images was arranged according to the previous publication [56].

For cell FISH experiments, whole chromosome probes XMP15 and XMP17 were hybridized following the manufacturer's protocol (MetaSystems), and nuclei were counterstained with DAPI. Pictures of the chromosomes were acquired by using Leica TCS SP8 WLL. Only the stained chromosomes were analyzed.

3D FISH and image analysis

Cells grown on glass slide for 2 h were fixed with 4% paraformaldehyde (PFA) for 15 min, permeabilized with 0.5% Triton X-100 in PBS for 20 min and then in 0.1 M HCl for 5 min. The cells were then washed with 2× SSC for 5 min twice and then washed in 50% formamide/4× SSC for 10 h at 4 °C. The hybridization was the same as mentioned above.

The images were acquired on Leica TCS SP8 WLL. For each imaging view, z-stacks covering the whole nuclei with a step size of 400 nm were taken for each channel and imaging conditions were kept for different views of one sample. DAPI was stained to represent the nuclear profile. The 3D image analysis was carried out in Imaris (Bitplane) by ImarisCell, a module designed specifically to identify, segment, track, measure and analyze cell, nucleus and vesicles in 3D images. For 3D chromosome FISH image analysis, "Surface" function was used to segment nuclear boundary by DAPI channel and chromosome territory boundary of Chr15 and Chr17 by 488 nm and 552 nm channel intensity, respectively. The volume and center of mass of nucleus and chromosome territories were output directly. The volume of each nucleus was measured to normalize the volume of chromosome territories. Distance between nuclear center of mass and chromosome territories was normalized by the cubic root of nuclear volume. We only selected haploid cells for chromosome FISH analyses.

Tissue FISH

The mice were euthanized by CO_2. The tissues were harvested and fixed in 4% PFA and embedded in paraffin. After dewaxing and rehydration, the tissue section slides were heated in ddH_2O for 25 min and digested with

pepsin (1 mg/mL in 10 mM HCl), and then washed in 50% formamide/4× SSC for 10 h at 4 °C. The XMP15 and XMP17 probes were added for hybridization at 80 °C for 4 min on a hot plate and then at 37 °C overnight in a humidified chamber. The glass coverslips were removed and the slides were washed in 0.1% tween 20/2× SSC at 37 °C for 5 min, and then 0.3% tween 20/0.4× SSC at 73 °C for 2.5 min. After draining, the slides were then washed in 0.1% tween 20/2× SSC at room temperature (RT) for 1.5 min. Subsequently, the slides were briefly rinsed in ddH_2O and then air-dried at RT. Finally, nuclei were counterstained with DAPI. Pictures of the chromosomes were acquired by using Leica TCS SP8 WLL.

Quantification of relative distance of chromosome territories to the nuclear center as well as the relative distance between chromosome territories was done with ImageJ software. The center and area of each nucleus and chromosome territory of Chr15 and Chr17 were measured. Relative distance between Chr15 and Chr17 was calculated as the shortest distance between two pairs of Chr15 and Chr17 in diploid cells and was normalized by the square root of nuclear area.

HE staining

Animals were sacrificed and tissues were harvested and fixed in 4% PFA, embedded in paraffin. After dewaxing and rehydration, tissue section slides were stained with hematoxylin stain solution (Yeasen) for 5 min and eosin Y stain solution (Yanye) for 10 s. The slides were dehydrated in increasing concentrations of alcohols, cleared by xylene, and mounted in neutral balsam. Pictures were taken by Olympus BX53.

Teratoma formation and IHC

The Diploid (2n) cells of haESCs were purified with FACS. Di-haESCs (approximately 1×10^7 cells) were trypsinized into single cells with PBS buffer and subcutaneously injected into BABL/c nude mice (4 weeks old). Ten mice were injected for each cell line. After 4–6 weeks, animals were sacrificed and teratomas were fixed in 4% PFA, embedded in paraffin.

For IHC, teratoma sections were blocked using 10% normal goat serum (Solarbio) in PBS for 1 h and stained with primary antibody at 4 °C overnight, followed by secondary antibody (SCBT) for 1 h at RT and DAB enhancer (MKbio). After hematoxylin staining for 2 min, the slides were dehydrated in increasing concentrations of alcohols, cleared by xylene, and mounted in neutral balsam. Pictures were taken by Olympus BX53.

The used primary antibody: anti-alpha-1-fetoprotein (ARG56134, Arigobio) at 1:500 dilution for endoderm lineage; anti-smooth muscle actin (sc-53142, SCBT) at 1:50 dilution for mesoderm lineage; anti-Tuj1 (sc-80005, SCBT) at 1:400 dilution for ectoderm lineage.

Measurements of blood parameters

The blood samples were collected into micro blood collection tubes by the retro-orbital bleeding in mice. Microtubes contained EDTA as anticoagulants were used for hematological examinations, and microtubes without EDTA were used for clinical chemistry serum measurements. Hematological parameters of all samples were analyzed on XN-1000V Hematology Analyzer (Sysmex). The clinical chemistry parameters glucose (GLU), total protein (TP), uric acid (URIC), albumin (ALB), triglyceride (TRIG), cholesterol (CHOL), chloride (Cl^-), sodium (Na^+), urea, calcium (Ca^{2+}), aspartate aminotransferase (AST), alkaline phosphatase (ALKP), alanine aminotransferase (ALT), lactate dehydrogenase (LDH), and high-density lipoproteins (HDL) were determined in the serum with a VITROS 4600 (Ortho Clinical Diagnostics).

Hi-C library preparation and sequencing

Cells were cross-linked with 3% fresh formaldehyde (final concentration) and then quenched with 0.15 M glycine (final concentration) for 5 min. Genomic DNA was extracted and digested with 200 units *Mbo*I (NEB)[57]. DNA ends were labeled with biotin-14-dCTP (TriLINK), and after ligated, they were sheared to a length of ~400 bp. Point ligation junctions were pulled down with Dynabeads MyOne Streptavidin C1 (Thermo). The Hi-C library for Illumina sequencing was prepared with the NEBNext Ultra II DNA Library Prep Kit for Illumina (NEB) according to the manufacturer's instructions. Paired-end sequencing (150 bp read length) was performed on the NovaSeq 6000 platform (Illumina) and 400 Gb raw reads were obtained. Paired-end sequencing reads were trimmed for adaptors and low-quality reads by fastp (v0.21.0) with default parameters[58]. Trimmed reads were processed using HiCExplorer (v3.7.2) as previously described[59]. Briefly, mates were mapped individually to Mouse genome GRCm39 using BWA (bwa-0.7.17) with the option 'mem -A 1 -B 4 -E 50 -L 0', the resulting BAM files were used to build contact matrices at binning resolutions of 20 Kb and 1 Mb. The raw contact matrices were normalized using a fast balancing algorithm introduced by Knight and Ruiz (KR)[60] to correct bias and scaled to a fixed read count defined by the sample with the lowest coverage. TADs were identified using command 'hicFindTADs' with default parameters, the resulting bedGraph files with insulation scores were processed by deepTools (v3.4.3) for further visualization [61].

Inferring the 3D structure of the genome

The 3D structure of the genome in WT and 25A cells were inferred using PASTIS v0.5 with the PM2 algorithm[62], the resulting Protein Data Bank files were visualized with Pymol (v2.4.0).

RNA-seq analysis

Total RNA was isolated from the cells using Trizol reagent (Ambion). The library preparation followed the standard procedure (Illumina). The libraries were sequenced on the Illumina NovaSeq 6000 platform using the 150 bp paired-end sequencing strategy. For each sample, 8 Gb clean data were obtained. The clean reads were mapped to the reference genome GRCm39 using STAR (v2.0), and the resulting BAM files were converted to genome-wide tracks using deepTools. Transcript quantification was performed using kallisto (v0.46.1) with default parameters, which was further processed by DESeq2 (v1.14.1) for differential expression with a FDR cutoff of 5%.

Embryonic bodies (EB) formation and differentiation of haESCs

Before EB formation, the dishes were coated with gelatin. The haESCs were trypsinized and diluted into 2.5×10^5 cells/mL in the differentiation medium (DM: DMEM with 20% FBS, non-essential amino acids, β-mercaptoethanol, L-glutamine, penicillin/streptomycin, and sodium pyruvate), and aliquoted into 20 μL drops on the lid of 10-cm culture dishes, and 50 drops in total following the standard hanging-drop method[63,64]. The droplets were collected from the lid on the next day and placed in 10-cm culture dishes filled with 10 mL DM and incubated at 37 °C. The EBs were harvested 5 d later and transferred onto a new 48-well (gelatin coated) at a density of 10 EBs per well in DM and refresh the DM every 2 d. The differentiated EBs were harvested on the 14th day.

Real-time PCR

Total RNA was extracted from the haESCs using TRIzol Reagent (Ambion). cDNA was generated by reverse transcription using Hiscript III RT supermix (Vazyme) according to the manufacturer's instructions. The pluripotency marker genes were quantified by Real-time PCR using AceQ Universal SYBR qPCR Master mix (Vazyme) and Roche LightCycler 96 qPCR Real-Time PCR system. Primers specific to each marker gene were listed in Supplementary Table S3.

Acknowledgements

We thank the department of embryo manipulation led by Mrs. Wei Tang for the ICAHCI and embryo transfer.

Author details

[1]State Key Laboratory of Cell Biology, Shanghai Institute of Biochemistry and Cell Biology, Center for Excellence in Molecular Cell Science, Chinese Academy of Sciences, University of Chinese Academy of Sciences, Shanghai, China. [2]State Key Laboratory of Molecular Biology, Shanghai Institute of Biochemistry and Cell Biology, Center for Excellence in Molecular Cell Science, Chinese Academy of Sciences, University of Chinese Academy of Sciences, Shanghai, China. [3]Key Laboratory of Systems Health Science of Zhejiang Province, School of Life Science, Hangzhou Institute for Advanced Study, University of Chinese Academy of Sciences, Hangzhou, China. [4]School of Life Science and Technology, ShanghaiTech University, Shanghai, China

Author contributions

J.-Q.Z. and Y.Z. conceived and supervised the project, analyzed the data, and drafted the manuscript. Y.W. constructed the chromosome fusion haESCs, carried out most of the experiments and data analyses, and drafted the manuscript. Z.Q. and Y.F. conducted IHC and some of the histological experiments and drafted the manuscript. Y.C. and J.Shi performed Hi-C and RNA-seq data analyses. J.P. and J.Song provided help with the histological experiments. J.L. provided the original haESCs and contributed to data analyses.

Funding

This research was supported by grants from the Strategic Priority Research Program of the National Key Research and Development Program of China (2019YFA0109902, 2020YFA0509000), the National Natural Science Foundation of China (32293232, 32130025, 32270787) and Chinese Academy of Sciences (ZDBS-LY-SM018).

Data availability

All data are available in the manuscript or supplementary materials.

Conflict of interest

The authors declare no competing interests.

Supplementary information The online version contains supplementary material available at https://doi.org/10.1038/s41421-022-00511-1.

Received: 15 November 2022 Accepted: 18 December 2022
Published online: 24 January 2023

References

1. Khandelwal, S. Chromosome evolution in the genus *Ophioglossum* L. *Bot. J. Linn. Soc.* **102**, 205–217 (1990).
2. Crosland, M. W. & Crozier, R. H. *Myrmecia pilosula*, an ant with only one pair of chromosomes. *Science* **231**, 1278 (1986).
3. Bolzer, A. et al. Three-dimensional maps of all chromosomes in human male fibroblast nuclei and prometaphase rosettes. *PLoS Biol.* **3**, e157 (2005).
4. Cheeseman, I. M. & Desai, A. Molecular architecture of the kinetochore-microtubule interface. *Nat. Rev. Mol. Cell Biol.* **9**, 33–46 (2008).
5. Bianchi, A. & Shore, D. How telomerase reaches its end: Mechanism of telomerase regulation by the telomeric complex. *Mol. Cell* **31**, 153–165 (2008).
6. O'Sullivan, R. J. & Karlseder, J. Telomeres: protecting chromosomes against genome instability. *Nat. Rev. Mol. Cell Biol.* **11**, 171–181 (2010).
7. Meaburn, K. J. & Misteli, T. Cell biology: chromosome territories. *Nature* **445**, 379–781 (2007).
8. Cremer, T. & Cremer, M. Chromosome territories. *Cold Spring Harb. Perspect. Biol.* **2**, a003889 (2010).
9. Cremer, T. & Cremer, C. Chromosome territories, nuclear architecture and gene regulation in mammalian cells. *Nat. Rev. Genet.* **2**, 292–301 (2001).
10. Lamond, A. I. & Earnshaw, W. C. Structure and function in the nucleus. *Science* **280**, 547–553 (1998).
11. Croft, J. A. et al. Differences in the localization and morphology of chromosomes in the human nucleus. *J. Cell Biol.* **145**, 1119–1131 (1999).
12. Cremer, M. et al. Non-random radial higher-order chromatin arrangements in nuclei of diploid human cells. *Chromosome Res.* **9**, 541–567 (2001).
13. Stevens, T. J. et al. 3D structures of individual mammalian genomes studied by single-cell Hi-C. *Nature* **544**, 59–64 (2017).
14. Tanabe, H. et al. Evolutionary conservation of chromosome territory arrangements in cell nuclei from higher primates. *Proc. Natl. Acad. Sci. USA* **99**, 4424–4429 (2002).

15. Branco, M. R. & Pombo, A. Intermingling of chromosome territories in interphase suggests role in translocations and transcription-dependent associations. *PLoS Biol.* **4**, e138 (2006).
16. Capanna, E. & Redi, C. A. Whole-arm reciprocal translocation (WART) between Robertsonian chromosomes: finding of a Robertsonian heterozygous mouse with karyotype derived through WARTs. *Chromosome Res.* **3**, 135–137 (1995).
17. Nachman, M. W. & Searle, J. B. Why is the house mouse karyotype so variable? *Trends Eco. Evol.* **10**, 397–402 (1995).
18. PiáLek, J., Hauffe, H. C. & Searle, J. B. Chromosomal variation in the house mouse. *Biol. J. Linn. Soc.* **84**, 535–563 (2005).
19. Garagna, S., Page, J., Fernandez-Donoso, R., Zuccotti, M. & Searle, J. B. The Robertsonian phenomenon in the house mouse: mutation, meiosis and speciation. *Chromosoma* **123**, 529–544 (2014).
20. Fontana, F. & Rubini, M. Chromosomal evolution in Cervidae. *Biosystems* **24**, 157–174 (1990).
21. Neitzel, H. In Cytogenetics, (eds. Obe, G. & Basler, A.) 90–112 (Springer, 1987).
22. Yin, Y. et al. Molecular mechanisms and topological consequences of drastic chromosomal rearrangements of muntjac deer. *Nat. Commun.* **12**, 6858 (2021).
23. Shao, Y. et al. Creating a functional single-chromosome yeast. *Nature* **560**, 331–335 (2018).
24. Luo, J., Sun, X., Cormack, B. P. & Boeke, J. D. Karyotype engineering by chromosome fusion leads to reproductive isolation in yeast. *Nature* **560**, 392–396 (2018).
25. Gu, X. et al. Single-chromosome fission yeast models reveal the configuration robustness of a functional genome. *Cell Rep.* **40**, 111237 (2022).
26. Zhong, C. et al. CRISPR-Cas9-mediated genetic screening in mice with haploid embryonic stem cells carrying a Gge RNA library. *Cell Stem Cell* **17**, 221–232 (2015).
27. Sharma, S. & Raghavan, S. C. In Encyclopedia of Cell Biology, (eds Bradshaw, R. & Stahl, P.) 451–455 (Academic Press, 2016).
28. Mayer, R. et al. Common themes and cell type specific variations of higher order chromatin arrangements in the mouse. *BMC Cell Biol.* **6**, 44 (2005).
29. Sun, H. B., Shen, J. & Yokota, H. Size-dependent positioning of human chromosomes in interphase nuclei. *Biophys. J.* **79**, 184–190 (2000).
30. Boyle, S. et al. The spatial organization of human chromosomes within the nuclei of normal and emerin-mutant cells. *Hum. Mol. Genet.* **10**, 211–219 (2001).
31. Cremer, M. et al. Inheritance of gene density-related higher order chromatin arrangements in normal and tumor cell nuclei. *J. Cell Biol.* **162**, 809–820 (2003).
32. Osborne, C. S. et al. Active genes dynamically colocalize to shared sites of ongoing transcription. *Nat. Genet.* **36**, 1065–1071 (2004).
33. Mahy, N. L., Perry, P. E. & Bickmore, W. A. Gene density and transcription influence the localization of chromatin outside of chromosome territories detectable by FISH. *J. Cell Biol.* **159**, 753–763 (2002).
34. Volpi, E. V. et al. Large-scale chromatin organization of the major histocompatibility complex and other regions of human chromosome 6 and its response to interferon in interphase nuclei. *J. Cell Sci.* **113**, 1565–1576 (2000).
35. Williams, R. R., Broad, S., Sheer, D. & Ragoussis, J. Subchromosomal positioning of the epidermal differentiation complex (EDC) in keratinocyte and lymphoblast interphase nuclei. *Exp. Cell Res.* **272**, 163–175 (2002).
36. Dixon, J. R. et al. Chromatin architecture reorganization during stem cell differentiation. *Nature* **518**, 331–336 (2015).
37. Nora, E. P. et al. Spatial partitioning of the regulatory landscape of the X-inactivation centre. *Nature* **485**, 381–385 (2012).
38. Dixon, J. R. et al. Topological domains in mammalian genomes identified by analysis of chromatin interactions. *Nature* **485**, 376–380 (2012).
39. Meaburn, K. J. et al. Tissue-of-origin-specific gene repositioning in breast and prostate cancer. *Histochem. Cell Biol.* **145**, 433–446 (2016).
40. Garagna, S., Zuccotti, M., Capanna, E. & Redi, C. A. High-resolution organization of mouse telomeric and pericentromeric DNA. *Cytogenetic. Genome Res.* **96**, 125–129 (2002).
41. Kalitsis, P., Griffiths, B. & Choo, K. H. Mouse telocentric sequences reveal a high rate of homogenization and possible role in Robertsonian translocation. *Proc. Natl. Acad. Sci. USA* **103**, 8786–8791 (2006).
42. Hudakova, S., Kunzel, G., Endo, T. R. & Schubert, I. Barley chromosome arms longer than half of the spindle axis interfere with nuclear divisions. *Cytogenetic. Genome Res.* **98**, 101–107 (2002).
43. Rens, W., Torosantucci, L., Degrassi, F. & Ferguson-Smith, M. A. Incomplete sister chromatid separation of long chromosome arms. *Chromosoma* **115**, 481–490 (2006).
44. Schubert, I. & Oud, J. L. There is an upper limit of chromosome size for normal development of an organism. *Cell* **88**, 515–520 (1997).
45. Szczepinska, T., Rusek, A. M. & Plewczynski, D. Intermingling of chromosome territories. *Genes Chromosomes Cancer* **58**, 500–506 (2019).
46. Spilianakis, C. G., Lalioti, M. D., Town, T., Lee, G. R. & Flavell, R. A. Interchromosomal associations between alternatively expressed loci. *Nature* **435**, 637–645 (2005).
47. Maass, P. G., Barutcu, A. R. & Rinn, J. L. Interchromosomal interactions: A genomic love story of kissing chromosomes. *J. Cell Biol.* **218**, 27–38 (2019).
48. Wang, L. B. et al. A sustainable mouse karyotype created by programmed chromosome fusion. *Science* **377**, 967–975 (2022).
49. Zhang, X. M. et al. Creation of artificial karyotypes in mice reveals robustness of genome organization. *Cell Res.* **32**, 1026–1029 (2022).
50. Hauffe, H. C. Giménez, M. & Searle, J. In Evolution of the House Mouse, (eds. Macholán, M., Baird, S., Munclinger, P. & Piálek, J.) 407–430 (Cambridge University Press, 2012).
51. Yang, H. et al. Generation of genetically modified mice by oocyte injection of androgenetic haploid embryonic stem cells. *Cell* **149**, 605–617 (2012).
52. Ying, Q. L. et al. The ground state of embryonic stem cell self-renewal. *Nature* **453**, 519–523 (2008).
53. Qu, C. et al. Haploid embryonic stem cells can be enriched and maintained by simple filtration. *J. Biol. Chem.* **293**, 5230–5235 (2018).
54. Leeb, M. & Wutz, A. Derivation of haploid embryonic stem cells from mouse embryos. *Nature* **479**, 131–134 (2011).
55. Zhong, C. et al. Parthenogenetic haploid embryonic stem cells efficiently support mouse generation by oocyte injection. *Cell Res.* **26**, 131–134 (2016).
56. Mann, J. R., Gadi, I., Harbison, M. L., Abbondanzo, S. J. & Stewart, C. L. Androgenetic mouse embryonic stem cells are pluripotent and cause skeletal defects in chimeras: implications for genetic imprinting. *Cell* **62**, 251–260 (1990).
57. Lieberman-Aiden, E. et al. Comprehensive mapping of long-range interactions reveals folding principles of the human genome. *Science* **326**, 289–293 (2009).
58. Chen, S., Zhou, Y., Chen, Y. & Gu, J. fastp: an ultra-fast all-in-one FASTQ preprocessor. *Bioinformatics* **34**, i884–i890 (2018).
59. Ramirez, F. et al. High-resolution TADs reveal DNA sequences underlying genome organization in flies. *Nat. Commun.* **9**, 189 (2018).
60. Knight, P. A. & Ruiz, D. A fast algorithm for matrix balancing. *IMA J. Numer. Anal.* **33**, 1029–1047 (2013).
61. Ramirez, F. et al. deepTools2: a next generation web server for deep-sequencing data analysis. *Nucleic Acids Res.* **44**, W160–W165 (2016).
62. Varoquaux, N., Ay, F., Noble, W. S. & Vert, J. P. A statistical approach for inferring the 3D structure of the genome. *Bioinformatics* **30**, i26–i33 (2014).
63. Boheler, K. R. et al. Differentiation of pluripotent embryonic stem cells into cardiomyocytes. *Circ. Res.* **91**, 189–201 (2002).
64. Wobus, A. M., Guan, K., Yang, H. T. & Boheler, K. R. Embryonic stem cells as a model to study cardiac, skeletal muscle, and vascular smooth muscle cell differentiation. *Methods Mol. Biol.* **185**, 127–156 (2002).